ResearchGate

See discussions, stats, and author profiles for this publication at: https://www.researchgate.net/publication/314230287

Hybrid RANS/LES simulations of the three-dimensional flow at root region of a 10 MW wind turbine rotor

Conference Paper · November 2016

CITATION
1

READS
60

4 authors:

Galih Bangga
Universität Stuttgart
35 PUBLICATIONS **84** CITATIONS
SEE PROFILE

Pascal Weihing
Universität Stuttgart
16 PUBLICATIONS **49** CITATIONS
SEE PROFILE

Thorsten Lutz
Universität Stuttgart
154 PUBLICATIONS **761** CITATIONS
SEE PROFILE

Ewald Krämer
Universität Stuttgart
200 PUBLICATIONS **812** CITATIONS
SEE PROFILE

Some of the authors of this publication are also working on these related projects:

Three Dimensional Effects in the Root Area of Wind Turbines View project

Hyperion Green Aircraft View project

All content following this page was uploaded by Galih Bangga on 03 July 2017.

The user has requested enhancement of the downloaded file.

Hybrid RANS/LES simulations of the three-dimensional flow at root region of a 10 MW wind turbine rotor

Galih Bangga, Pascal Weihing, Thorsten Lutz and Ewald Krämer

Abstract Numerical computations using the Unsteady Reynolds Averaged Navier-Stokes (URANS) and Delayed Detached-Eddy Simulations (DDES) approaches are carried out to investigate the complex three-dimensional flow in the root region of a generic 10 MW wind turbine rotor. Preliminary studies regarding the time step size and the number of rotor revolution required for the time averaging procedure are conducted. In the blade outer region, URANS is sufficient to predict the general flow characteristics, but small discrepancies are observed in the blade root area where the flow is massively separated.

1 Introduction

A large demand of electricity and increasing public awareness towards environmental friendly energy sources have led to rapid development of wind turbines. To fulfil these needs, two options can be used: (1) establish more wind farms or (2) increase the turbine size to enhance the power production of each turbine. With many technical constraints involved, direct up-scaling of the turbine is not desirable for wind turbine rotors above 10 MW because the aerodynamic and structural behaviors of these machines are not well understood. The current state of the art aerodynamic tools are not yet well validated for these large wind turbine rotors [17]. Furthermore, the increasing wind turbine size enforces the use of much thicker airfoils in the inboard area, extending further outboard longer than the smaller rotors, to provide the necessary structural stability. This is not desirable as the thick airfoils often deteriorate the aerodynamic performance. Baker *et al.* [2] and Bangga *et al.* [5] documented that thicker airfoils tend to have a lower lift to drag ratio and earlier stall, especially under soiled (tripped) conditions.

G. Bangga, P. Weihing, T. Lutz and E. Krämer
Institute of Aerodynamics and Gas Dynamics (IAG), University of Stuttgart, Pfaffenwaldring 21 Stuttgart 70569, Germany, e-mail: bangga@iag.uni-stuttgart.de

This article has been accepted in the Springer book: *Notes on Numerical Fluid Mechanics and Multidisciplinary Design* as a contribution in the STAB 2016 Symposium, Braunschweig, Germany. The book chapter will be published in 2017.

It was widely documented [2, 3, 5, 18–23] that URANS hardly predicts the flow characteristics of airfoils in the post stall conditions. Unfortunately, even the use of the most modern turbulence models could not essentially improve the situation [7,8]. Baker *et al.* [2] and Bangga *et al.* [5] showed that the maximum lift coefficient of the inboard airfoil is overpredicted in their CFD simulations. The fluid flow in the blade inboard region is highly complex and not well understood. The complexity stems from the combinations of massive flow separation at high angle of attack and three-dimensional effects due to blade rotation. Many attempts using RANS simulations have been carried out for this issue, but most of the results were inaccurate at high wind speed case under stalled conditions.

Large Eddy Simulations (LES) offer a better prediction for massively separated flow field, but the computational cost is way more expensive than RANS. The idea of the hybrid RANS/LES technique, also known as Detached-Eddy Simulations (DES), is to design a turbulence model such that it works as a RANS model within the boundary layer, in order to save computational time, while working in the outer flow regime as a sub-grid-scale model to resolve the dominant turbulent structures in LES mode [24]. By doing so, the 3D flow characteristics are better captured while the computational cost can be kept small. It has been shown by Johansen *et al.* [10] that DES calculations were able to resolve more 3D flow structures near the blade root compared to RANS which allowed a better examination on the 3D effects. Using the same turbine, Li *et al.* [14] confirmed this observation for the NREL Phase VI rotor.

On this basis, the present study aims to obtain a better insight into the 3D effects for large turbines by employing the capability of DDES for separated flow. The preliminary study on the temporal resolution is presented in Section 3.1. The results are compared with the URANS simulations and detailed examinations are presented in Section 3.2. The investigation is then concluded in Section 4.

2 Computational Methods

2.1 Turbulence Modelling

In the present study, the turbulence is modelled by the Delayed Detached-Eddy Simulations (DDES) approach [21]. The method was developed to prevent the occurrence of the Modeled-Stress Depletion (MSD) and Grid-Induced Separation (GIS) [20] for ambiguous grid size usually observed in the original DES method [19]. The idea is similar to the boundary layer shielding approach proposed by Menter and Kuntz [15]. The DDES formulation is general and applicable to any turbulence model that involves an eddy viscosity [21]. This is done by revising the definition of the DES length scale (l_{DDES}) in DES97 as [18]

$$l_{DDES} = l_{RANS} - f_d \max\left[0, (l_{RANS} - l_{LES})\right], \tag{1}$$

This article has been accepted in the Springer book: *Notes on Numerical Fluid Mechanics and Multidisciplinary Design* as a contribution in the STAB 2016 Symposium, Braunschweig, Germany. The book chapter will be published in 2017.

In order to create a shielding of the boundary layer, the defined DDES length scale is coupled with the RANS model through l_{RANS}, where $l_{RANS} = k^{1/2}/(C_\mu \omega)$ depends on the turbulent kinetic energy (k), its specific dissipation rate (ω) and a constant (C_μ). The delaying function is defined as $f_d = 1 - \tanh[(8r_d)^3]$ and the quantity of r_d is defined as

$$r_d = \frac{\nu + \nu_t}{\kappa^2 d_w^2 \max\left[\left[\Sigma_{ij}(\partial u_i/\partial x_j)^2\right]^{1/2}, 10^{-10}\right]}, \tag{2}$$

where ν and ν_t are the laminar and turbulent viscosities, respectively, κ is the Kármán constant and d_w defines the wall distance. This variable is zero in a free shear flow and unity in a log layer [18]. In the present studies, the near wall RANS model uses the Menter SST turbulence model [16].

2.2 Test Cases and Computational Setup

The 10 MW rotor studied in this paper is the AVATAR blade [13] developed based on the DTU 10 MW wind turbine [1]. The aim is to model the aerodynamic characteristics of turbines larger than 10 MW with similar accuracy as is done for commercially sized turbines today [17]. The axial induction factor a is reduced to below 1/3, lying within $0.23 < a < 0.28$ which is better from a cost of energy point of view [17]. This design concept is denoted as low induction rotor or LIR concept. The chosen rated wind speed for this turbine is 10.75 m/s. The factor of 1.15 in radial direction is used to scale the original DTU 10 MW wind turbine by maintaining the output power to be the same, resulting to a radius of $R = 102.9$ m. In the present study, two different wind speeds, near the rated and under stalled conditions, are examined: U_∞ = 10.5 m/s and 20 m/s, respectively. The rotational speed and the pitch angle were kept constant at 9.02 rpm ($\Omega \approx 0.94$ rad/s) and 0°, respectively, in order to obtain different angles of attack α for the blade sections with the variation of the wind speeds. No tower was considered in these studies to isolate the resulting 3D flow field from the unsteady tower disturbances.

The CFD simulations presented in this paper were carried out using the block-structured solver FLOWer from the German Aerospace Center (DLR) [12]. The code was continuously developed for wind turbine applications during the last years at the Institute of Aerodynamics and Gas Dynamics - University of Stuttgart [8]. The Jameson-Schmidt-Turkel (JST) [9] finite volume formulation method with second order accuracy on smooth meshes is used. Dual time-stepping with second-order accuracy in time, multi-grid level 2 and the implicit residual smoothing with variable coefficients were applied [12].

The simulations are performed by modelling only one blade assuming flow periodicity. A uniform inflow condition is imposed at the farfield boundary. The computational domain size is set to 2000 m x 2000 m in streamwise (X) and crossflow (Z) directions, respectively, and the center of rotation is located at the origin. It

This article has been accepted in the Springer book: *Notes on Numerical Fluid Mechanics and Multidisciplinary Design* as a contribution in the STAB 2016 Symposium, Braunschweig, Germany. The book chapter will be published in 2017.

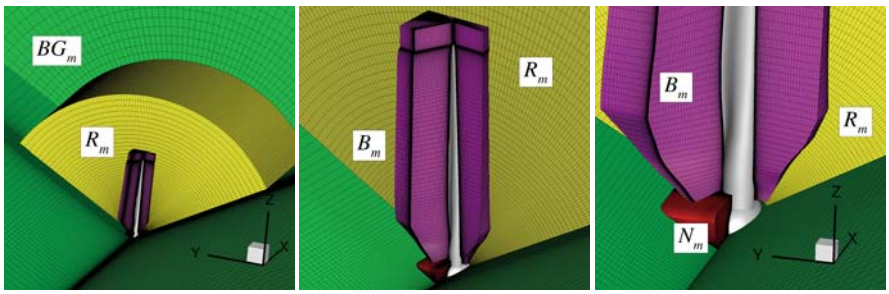

Fig. 1: Meshes used in the simulations. BG_m (green), R_m (yellow), B_m (purple), and N_m (red) represent the background, wake refinement, blade and nacelle meshes, respectively. X, Y and Z are the inertial coordinate system.

shall be noted that the shape of the domain is 1/3 of cylinder (Figure 1). The grid consists of several components: background (BG_m), wake refinement (R_m), blade (B_m) and nacelle (N_m) meshes, shown in Figure 1. The blade mesh uses the C-H topology with the resolution of 280x128x192 cells in chordwise, normal and radial directions, respectively. The non-dimensional wall distance of all the components is set to meet $y^+ < 1$ as no wall function is employed. A grid number of 32 cells is located across the boundary layer. A grid dependency study for this blade mesh was carried out in [6], implying that the present blade mesh resolution is sufficient to predict the sectional loads. The cell size of the wake refinement mesh (R_m) is 1 m at the tip location, and becomes finer closer to the root area. The cells number of this specific grid component reaches 16.3 million, while the total number of cells for all the grid components is 32.7 million. This resolution was observed to sufficiently capture the vortex development downstream of the turbine by Kim *et al.* [11]. The overset (Chimera) method is used which allows the mesh of each component to be built separately, simplifying the mesh generation significantly.

3 CFD Results

3.1 Dependency of the DDES Results upon Time-step Sizes

In this section, the dependency of the DDES solutions towards variation of the time step size, Δt = 1° to 3°, is examined for the 10.5 m/s wind speed case. It is worthwhile to mention that the relation between the time steps in [°] and in [s] is given by $\Delta t[\mathrm{s}] = \Delta t[^\circ]/(\Omega 360^\circ)$. At first, the calculations were performed up to 10 blade revolutions until the wake is fully developed. Then, the simulations were restarted from this conditions. In Figures 2 and 3, there are shown that the mean sectional loads and their frequency spectra for various rotor revolutions ($R1$ - $R6$) are similar. It shall be

This article has been accepted in the Springer book: *Notes on Numerical Fluid Mechanics and Multidisciplinary Design* as a contribution in the STAB 2016 Symposium, Braunschweig, Germany. The book chapter will be published in 2017.

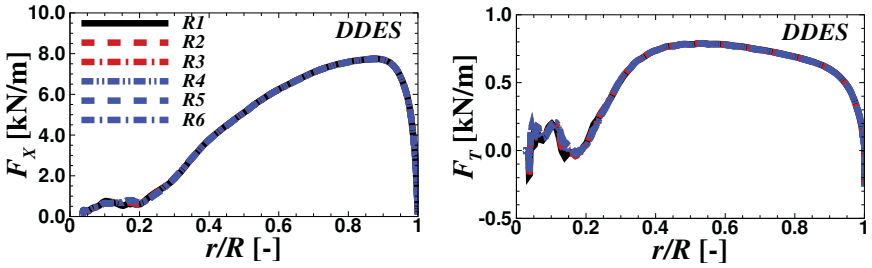

Fig. 2: Time-averaged sectional loads over one ($R1$) up to six rotor revolutions ($R6$). The time averaging uses the standard averaging procedure, *i.e.,* the sum of all values divided by the number of data. F_X and F_T indicate the rotor axial and tangential forces, respectively.

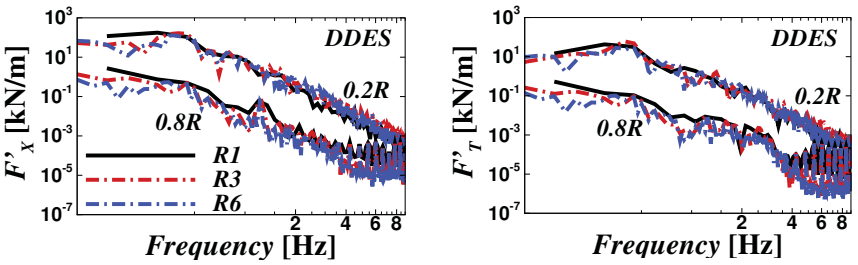

Fig. 3: Frequency spectra of the sectional loads over one ($R1$) up to six rotor revolutions ($R6$). F_X and F_T indicate the axial and tangential force amplitudes, respectively.

noted that the time averaging was carried out by excluding the first 10 revolutions. This means that $R1$ is for 11 (10+1) rotor revolutions, $R3$ for 13 (10+3) and $R6$ for 16 (10+6). With increasing number of revolutions, the solutions are converged at a certain value with little variation over each revolution. It is shown in Figure 3 that the amplitude for $R1$ is smaller in the blade inboard region and a bit higher in the outer blade sections compared to $R3$ and $R6$, but the general trend of the spectra is similar. Therefore, time-averaging over one revolution ($R1$) is sufficient and applied for the rest of the simulations.

Figure 4 shows that the tangential force predicted by DDES varies depending on the used time step size, especially in the blade inboard region ($r/R < 0.3$). The convergence seems to be achieved for $\Delta t = 2°$. This time step size is then used for further simulations. The small difference in the blade inboard region is caused by the finer re-

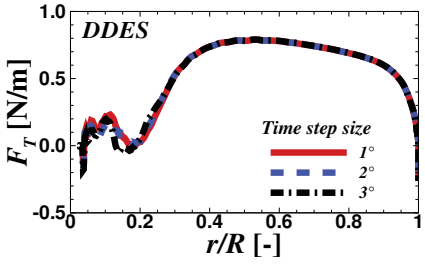

Fig. 4: Time-averaged tangential force for various time step sizes.

This article has been accepted in the Springer book: *Notes on Numerical Fluid Mechanics and Multidisciplinary Design* as a contribution in the STAB 2016 Symposium, Braunschweig, Germany. The book chapter will be published in 2017.

solved flow structures for the smaller time step. This happens because the time step size becomes much smaller than the convective time of a fluid particle passing the local airfoil section, defined by $\Delta t_c = c/V$, where c and V are the local chord length and kinematic velocity, defined as $V = (U_\infty^2 + (\Omega r)^2)^{0.5}$. The convective time scale depends on the operating conditions of the rotor. In the outer region, the tangential force almost coincides each other due to two main reasons. (1) The flow is attached so that the smaller time step does not improve the solutions. (2) The fine turbulent scales due to flow unsteadiness are not accurately captured in the simulations as the time step size is of the order of the flow convective time. For example, the convective time near the tip is about $\Delta t_c = 3.46^\circ$ that the ratio of $\Delta t/\Delta t_c$ is about 28.9% (for $\Delta t = 1^\circ$). At r/R = 0.2, the ratio becomes considerably smaller ($\Delta t/\Delta t_c$ = 1.06%) as the kinematic velocity is smaller. Furthermore, it has been shown by Bangga *et al.* [4, 6] that the flow was massively separated in the blade root region. It was further observed that a strong radial flow occurs within the separation area causing remarkable 3D effects.

3.2 Comparison with URANS

The comparison between the URANS and DDES computations for the AVATAR blade with the same near wall turbulence model, namely the Menter SST $k-\omega$ [16] is discussed in this section. The wake structures downstream of the rotor is shown in Figure 5. It can be seen that the size of the flow structures using both methods are very similar. According to [23], DES simulations require different numerical set-up than RANS. However, Waldmann *et al.* [22] documented that DES and URANS clearly showed different results even though the set-up was the same. On this basis, a more detailed exploration needs to be conducted. Figure 6 (left) shows the enlarged view of the flow topology near the turbine around the root area. It reveals that

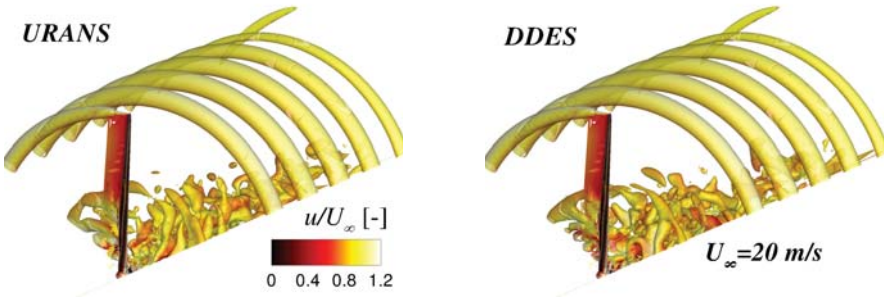

Fig. 5: Wake structures of the AVATAR rotor visualized by the λ_2 = -0.0827 s^{-2} iso-surface predicted by URANS and DDES for Δt = 2°.

This article has been accepted in the Springer book: *Notes on Numerical Fluid Mechanics and Multidisciplinary Design* as a contribution in the STAB 2016 Symposium, Braunschweig, Germany. The book chapter will be published in 2017.

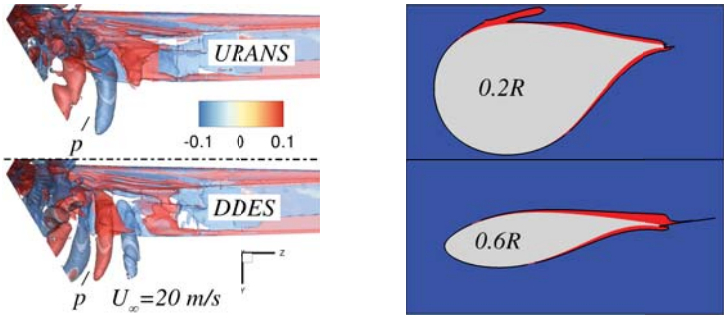

Fig. 6: Trailing vortex structures in the blade inboard region colored by the vorticity in Y-direction [1/s], λ_2 = -0.827 s^{-2} (left). Representation of the RANS (red) and LES (blue) zones around the blade sections at $r/R = 0.2$ and 0.6 (right).

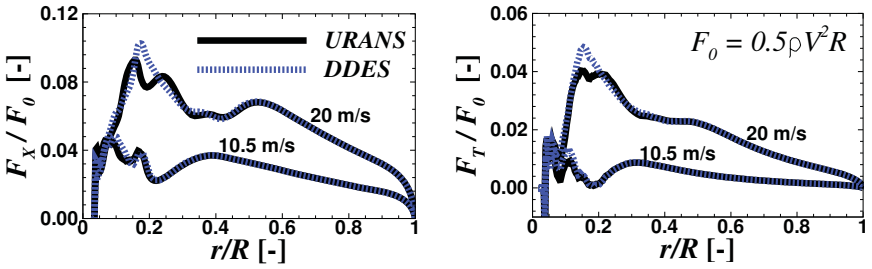

Fig. 7: Nondimensional sectional loads using two different turbulence models. V represents the local kinematic velocity, R is the rotor radius and ρ is the air density. F_X and F_T indicate the rotor axial and tangential forces, respectively.

the DDES prediction of the trailing vortex system slightly differs to the URANS results. DDES predicts stronger counter-rotating trailing vortices with opposing direction compared to URANS near the location marked by ***p*** (at $r/R \approx 0.17$), see Figure 6 (left). The discrepancies arise because massive flow separation is occurred in the blade inboard area. In this situation, the DDES capability in resolving flow structures using LES outside of the boundary layer takes its advantage. Figure 6 (right) illustrates that LES is properly employed outside of the boundary layer (blue color) and RANS is applied near the wall (red color). Furthermore, as discussed above, the time step size is reasonably small enough compared to the convective time scale in the blade inboard area ($\Delta t/\Delta t_c$ = 1.06% for $r/R = 0.2$) that an appropriate DDES computation can be performed. However, finding the time step limit where DDES is applicable is not part of the present works, and is recommended for future studies.

The trailing vortices in Figure 6 are the results of the radial load distributions shown in Figure 7. Any variation of the loads influences the strength of the inboard vortex. It can be seen that the sectional loads (F_X and F_T) increase locally

This article has been accepted in the Springer book: *Notes on Numerical Fluid Mechanics and Multidisciplinary Design* as a contribution in the STAB 2016 Symposium, Braunschweig, Germany. The book chapter will be published in 2017.

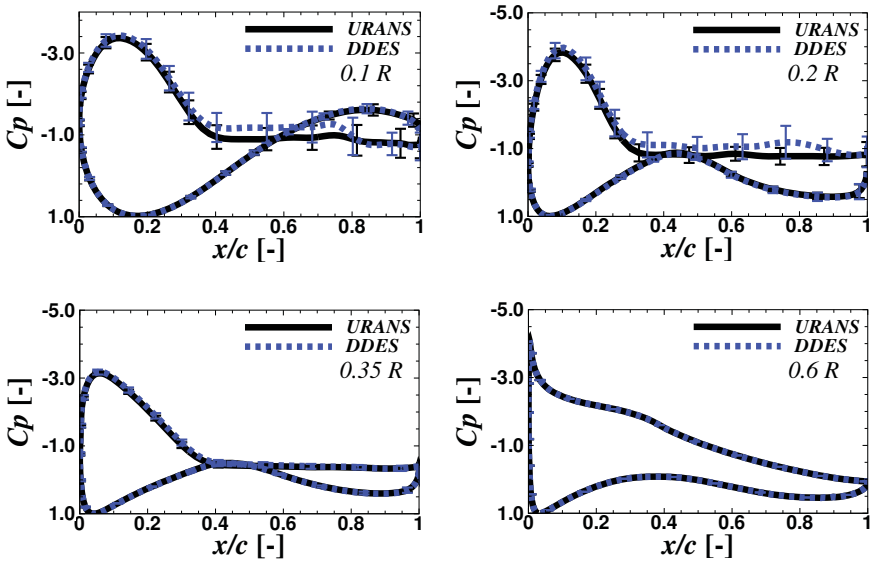

Fig. 8: Cp distributions at various radial stations for $U_\infty = 20$ m/s. The error bars indicate the standard deviation of the unsteady fluctuations.

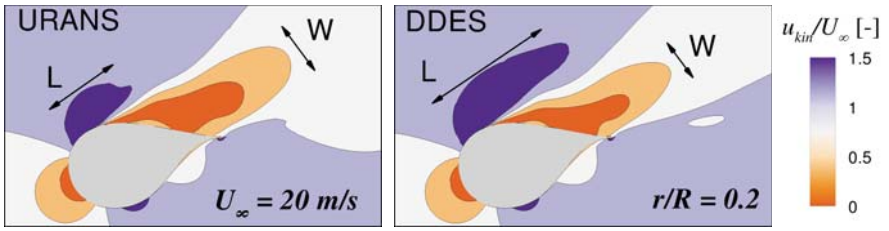

Fig. 9: Time-averaged kinematic streamwise velocity contour. W and L indicate the width of the separation area and the length of the accelerating flow region, respectively.

at $r/R = 0.17$, especially for the wind speed case of 20 m/s. This implies that the counter-rotating vortices near point ***p*** become stronger with increasing wind speed. Additionally, DDES predicts locally higher loads than URANS at this position. As a consequence, the vortical structures for the DDES simulations are also stronger than for the URANS results around this area, see Figure 6 (left).

Figure 8 demonstrates how the turbulence models affect the characteristics of Cp distribution for some selected radii. As already expected, DDES improves the CFD predictions only within the massively separated flow region, i.e., the pressure distributions are identical for attached and mildly separated flows (0.35R and 0.6R). The deviations occur within the separation area where DDES shows a smaller pressure

This article has been accepted in the Springer book: *Notes on Numerical Fluid Mechanics and Multidisciplinary Design* as a contribution in the STAB 2016 Symposium, Braunschweig, Germany. The book chapter will be published in 2017.

compared to URANS. It can be also seen that a noticeable deviation between DDES and URANS happens only when a strong unsteadiness occurs on the flow, as illustrated by the error bars in Figure 8 at $r/R = 0.1$ and 0.2. Figure 9 illustrates the flow field creating the pressure distribution of the blade section at $0.2R$. The streamwise velocity field is non-dimensionalized by the wind speed ($U_\infty = 20\ m/s$). Generally, the flow fields predicted by DDES and URANS are similar, but some discrepancies are observed on the suction side of the airfoil. It can be seen that the width of the separation area, indicated by letter ***W***, for DDES is smaller than for URANS. As a result, the vertical displacement of the separation area is narrower than in the URANS prediction, that facilitates the flow to be accelerated further downstream, indicated by letter ***L***. These cause DDES to predict a smaller pressure than URANS in the Cp distribution. Accordingly, the higher sectional loads at this position are observed in Figure 7.

4 Conclusion

Numerical simulations for the AVATAR rotor have been carried out using delayed detached-eddy simulations and Reynolds averaged Navier-Stokes approaches. A study on the impact of the number of blade revolutions and time-step (Δt) size were conducted. The simulations were carried out for 11 (10+1) rotor revolutions. The data extraction was performed only for the last one revolution, that is sufficient to capture the sectional loads and their frequency spectra. The chosen time step size of the studies is of $\Delta t = 2^\circ$. Comparison with URANS demonstrate that DDES does not significantly improve the sectional load predictions if the mesh and time step resolutions use the RANS set-up. It is observed that URANS is sufficient for the wind turbine prediction if no massive separation is encountered. On the other hand, the discrepancies between the used turbulence models are observed in the root region where the flow is separated with a strong unsteady fluctuation. For future studies, it is recommended to evaluate the limit of the ratio between the employed time step to the local convective time scale for a proper DDES computation.

Acknowledgements The authors gratefully acknowledge Ministry of Research, Technology and Higher Education of Indonesia, the AVATAR project and the HLRS computing center.

References

1. Bak, C., Zahle, F., Bitsche, R., Kim, T., et al.: Design and performance of a 10 mw turbine. Tech. rep., Technical University of Denmark, dtu-10mw-rwt.vindenergi.dtu.dk (2013)
2. Baker, J., Mayda, E., Van Dam, C.: Experimental analysis of thick blunt trailing-edge wind turbine airfoils. Journal of Solar Energy Engineering **128**(4), 422–431 (2006)
3. Bangga, G., Hutomo, G., Wiranegara, R., Sasongko, H.: Numerical study on a single bladed vertical axis wind turbine under dynamic stall. Journal of Mechanical Science and Technology **31**(1), 261–267 (2017)

4. Bangga, G., Kim, Y., Lutz, T., Weihing, P., Krämer, E.: Investigations of the inflow turbulence effect on rotational augmentation by means of CFD. Journal of Physics: Conference Series **753**(2), 022,026 (2016)
5. Bangga, G., Lutz, T., Krämer, E.: Numerical investigation of unsteady aerodynamic effects on thick flatback airfoils. In: Proceedings of German Wind Energy Conference 12, DEWEK 2015. Bremen, Germany (May 19-20, 2015)
6. Bangga, G., Lutz, T., Krämer, E.: An examination of rotational effects on large wind turbine blades. In: EAWE PhD Seminar 11. Stuttgart, Germany (September 23-25, 2015)
7. Bangga, G., Sasongko, H.: Dynamic stall prediction of a pitching airfoil using an adjusted two-equation URANS turbulence model. Journal of Applied Fluid Mechanics **10**(1), 1–10 (2017)
8. Bangga, G., Weihing, P., Lutz, T., Krämer, E.: Effect of computational grid on accurate prediction of a wind turbine rotor using delayed detached-eddy simulations. Journal of Mechanical Science and Technology **31**(5) (2017)
9. Jameson, A., Schmidt, W., Turkel, E., et al.: Numerical solutions of the euler equations by finite volume methods using runge-kutta time-stepping schemes. AIAA paper **1259**, 1981 (1981)
10. Johansen, J., Sorensen, N., Michelsen, J., Schreck, S.: Detached-eddy simulation of flow around the NREL phase VI blade. In: ASME 2002 Wind Energy Symposium, pp. 106–114. American Society of Mechanical Engineers (2002)
11. Kim, Y., Jost, E., Bangga, G., Weihing, P., Lutz, T.: Effects of ambient turbulence on the near wake of a wind turbine. Journal of Physics: Conference Series **753**(3), 032,047 (2016)
12. Kroll, N., Rossow, C.C., Becker, K., Thiele, F.: The megaflow project. Aerospace Science and Technology **4**(4), 223–237 (2000)
13. Lekou, D., Chortis, D., Chaviaropoulos, P., Munduate, X., Irisarri, A., et al.: Avatar deliverable d1.2 reference blade design. Tech. rep., ECN Wind Energy (2015)
14. Li, Y., Paik, K.J., Xing, T., Carrica, P.M.: Dynamic overset cfd simulations of wind turbine aerodynamics. Renewable Energy **37**(1), 285–298 (2012)
15. Menter, F., Kuntz, M.: Adaptation of eddy-viscosity turbulence models to unsteady separated flow behind vehicles. In: The aerodynamics of heavy vehicles: trucks, buses, and trains, pp. 339–352. Springer (2004)
16. Menter, F.R.: Two-equation eddy-viscosity turbulence models for engineering applications. AIAA journal **32**(8), 1598–1605 (1994)
17. Schepers, J., Ceyhan, O., Savenije, F., Stettner, M., et al.: Avatar: Advanced aerodynamic tools for large rotors. In: Proceedings of 33rd ASME Wind Energy Symposium (2015)
18. Shur, M.L., Spalart, P.R., Strelets, M.K., Travin, A.K.: A hybrid rans-les approach with delayed-des and wall-modelled les capabilities. Int. J. Heat Fluid Fl. **29**(6), 1638–1649 (2008)
19. Spalart, P., Jou, W., Strelets, M., Allmaras, S., et al.: Comments on the feasibility of les for wings, and on a hybrid rans/les approach. Advances in DNS/LES **1**, 4–8 (1997)
20. Spalart, P.R.: Detached-eddy simulation. Annual review of fluid mechanics **41**, 181–202 (2009)
21. Spalart, P.R., Deck, S., Shur, M., Squires, K., et al.: A new version of detached-eddy simulation, resistant to ambiguous grid densities. Theoretical and computational fluid dynamics **20**(3), 181–195 (2006)
22. Waldmann, A., Gansel, P.P., Lutz, T., Krämer, E.: Unsteady wake of the nasa common research model in low-speed stall. Journal of Aircraft pp. 1–14 (2015)
23. Weihing, P., Letzgus, J., Bangga, G., Lutz, T., Krämer, E.: Hybrid rans/les capabilities of the flow solver flower - application to flow around wind turbines. In: 6th Symposium on Hybrid RANS-LES Methods. Strasbourg, France (September 26 - 28, 2016)
24. Weihing, P., Meister, K., Schulz, C., Lutz, T., Krämer, E.: Cfd simulations on interference effects between offshore wind turbines. Journal of Physics: Conference Series **524**(1), 012,143 (2014)

View publication stats